Green and Highly Efficient MIMO Transceiver System for 5G Heterogenous Networks

Yasir I. A. Al-Yasir, Ahmed M. Abdulkhaleq, Naser Ojaroudi Parchin, Issa T. Elfergani, Jonathan Rodriguez, James M. Noras, Raed A. Abd-Alhameed, Ashwain Rayit, Rami Qahwaji

Abstract

The paper presents the general requirements and an exemplary design of the RF front-end system that in today´s handset is a key consumer of power. The design is required to minimize the carbon footprint in mobile handsets devices, whilst facilitating cooperation, and providing the energy-efficient operation of multi-standards for 5G communications. It provides the basis of hardware solutions for RF front-end integration challenges and offers design features covering energy efficiency for power amplifiers (PAs), Internet of Things (IoT) controlled tunable filters and compact highly isolated multiple-input and multiple-output (MIMO) antennas. An optimum design requires synergetic collaboration between academic institutions and industry in order to satisfy the key requirements of sub-6 GHz energy-efficient 5G transceivers, incorporating energy efficiency, good linearity and the potential for low-cost manufacturing. A highly integrated RF transceiver was designed and implemented to transmit and receive a picture using compact MIMO antennas integrated with efficient tunable filters and high linearity PAs. The proposed system has achieved a bit error rate (BER) of less than 10^{-10} at a data rate of 600 Mb/s with a wireless communication distance of more than 1 meter and power dissipation of 18-20 mW using hybrid beamforming technology and 64-QAM modulation.

Keywords: Multiple Input and Multiple Output (MIMO), sub-6 GHz, 5G, Energy-Efficient Transceivers, Internet of Things, Compact Antennas, Tunable filters, Power Amplifiers.

I. Introduction

5G RF front-ends for all wireless-enabled products are driven by cost, power efficiency, and available space within the unit. They are required to be compact, highly efficient, and able to be manufactured in large quantities to meet fast-growing global demand. In particular, 5G RF front-ends will play a major role in the Internet of Things (IoT) scenarios and devices, which require a minimum number of components, and scalability to address manufacturing in large volumes to reduce per-unit cost. In the current environment, most IoT devices are being built with low-cost parts originally developed for high-volume mobile phone production [1-2].

As we move toward 5G, the complexity of the RF front-end continues to increase. For instance, in addition to the main antenna path modules, diversity antennas provide both link robustness and increased downlink data rates. Designers are increasingly using receive diversity modules to process the diversity path, constituting receive (Rx) filters and increasingly incorporating amplifiers. Wireless carriers demanding higher 5G data rates drive carrier aggregation, creating more potential interference [3-4]. With almost all the available spectrum below 6 GHz now allocated, carriers will be forced to move to a higher frequency spectrum to secure bandwidth. As frequencies increase, RF propagation is reduced and penetration into buildings suffers: bandwidths available above 6 GHz lend themselves to short-range, point-to-point, and line-of-sight connections (likely in-building) [5-6]. 5G is expected to operate in two frequency bands including sub 6 GHz and millimetre-wave (mmW). It is also a balancing point between coverage and capacity that provides the perfect environment for the earliest 5G connectivity. However, the 3.4 to 3.8 GHz frequency band has been identified as a worthy candidate for 5G communications as recommended by the office of communication (Ofcom) [7].

In this context, the EU-funded H2020-MSCA project "SECRET" aims to provide a system-level solution for 5G and beyond, based on the notion of virtualization, that extends the virtualization coverage beyond the mobile networking infrastructure to include mobile and fixed terminals. This will open a plethora of new opportunities in the IoT world such as dynamic IoT networks set-up on-demand based on local decision making, storage, and connectivity enabling fast reaction time, and more efficient use of IoT radio resources. The SECRET scenarios provide the design requirements for 5G RF front-ends, which include energy-efficient and multi-standard RF elements for next-generation handsets, small base stations and IoT devices [8]. The proposed model of the small SECRET base station is based on subarray operations and the small SECRET user terminal array for MU-MIMO operation as shown in Figure 1. The physical and virtual beamforming harnesses various methodologies to generate the required weights to increase the signal-to-noise ratio and reduce the interference introduced due to the distribution of the virtual beams. A detailed model of the Mu-MIMO shown in Figure 1 in terms of beamforming diagrams and radio chains is illustrated in Figure 2. This shows how the front-end elements are connected to support hybrid beamforming, and the RF chains which deliver state-of-the-art IoT-controlled reconfigurability at the transmitter and receiver ends.

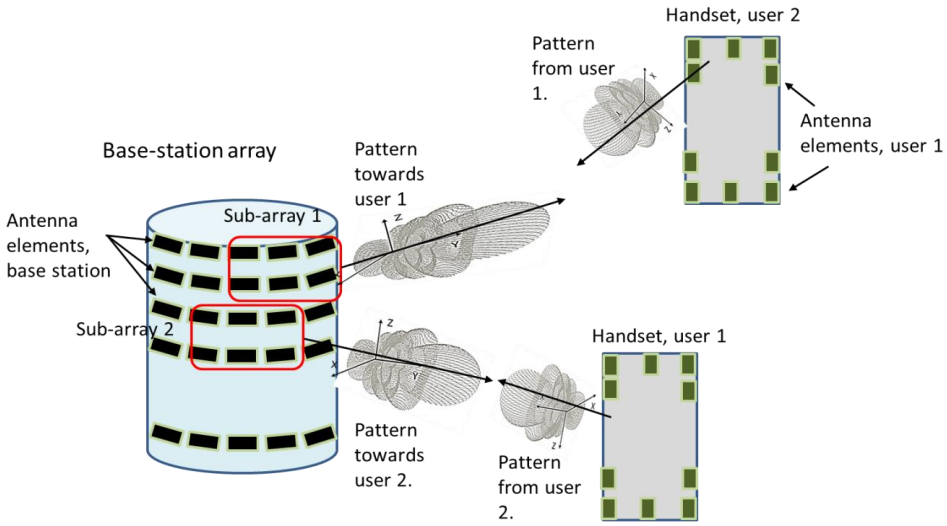

Figure 1: The proposed base station and user terminal arrays for Mu-MIMO.

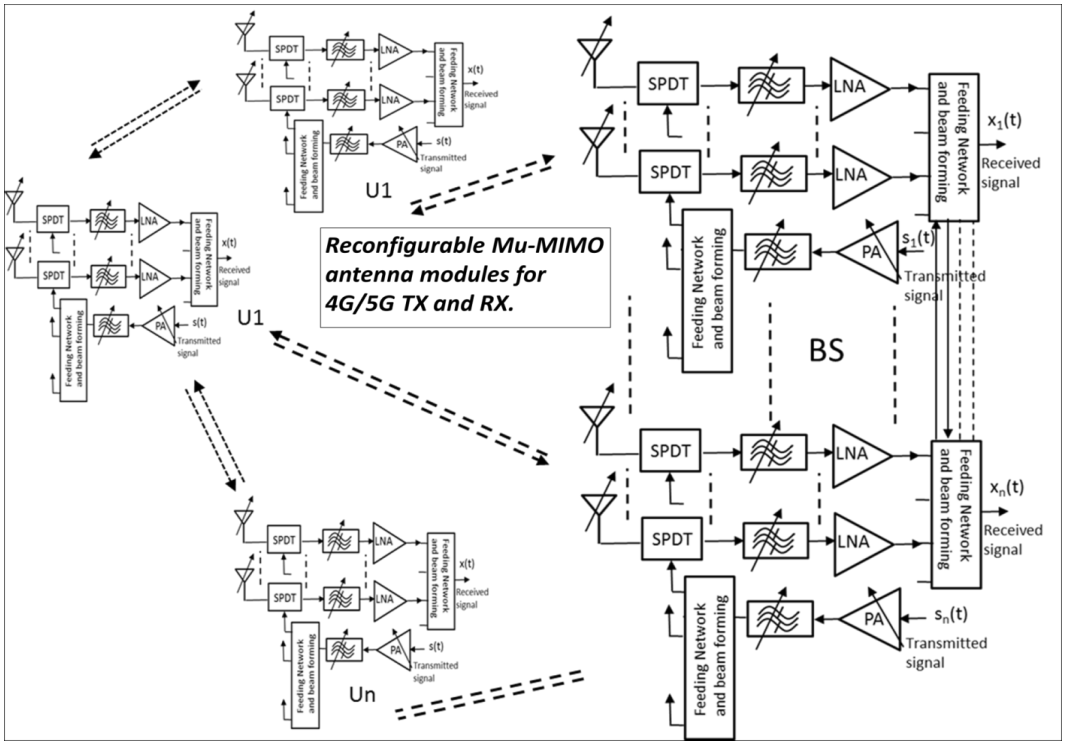

Figure 2: Reconfigurable Mu-MIMO modules for 4G/5G T_X and R_X.

In the literature, some works are devoted to the study of the heterogeneous transceiver architectures [9-18]. In [9], a 3.7–4.3 GHz frequency-modulated ultra-wideband (UWB) transceiver with analog reconfigurable subcarrier modulation index, UWB bandwidth and RF band is proposed. The introduced transceiver design including UWB bowtie antenna structures obtained a bit error rate (BER) of 10^{-6} at a data rate of 12.5 kb/s with a communication distance of 60 cm and the power dissipation of 21 mW with low cost and high robustness. A half-rate clock-embedded source-synchronous signaling arrangement to detect its constraints and to optimize the transceiver architecture in the existence of a band-limited channel is proposed in [10]. The prototype transceiver achieved a wide operating frequency range of 2.3–5 and 6–8 Gb/s, respectively, with a bit error rate of 10^{-12} and power efficiency that measured at maximum data rates was around 5 mW/Gb/s. Furthermore, to enable high data rates in mobile communication systems, the long-term evolution (LTE) standard has considered carrier aggregation (CA) to increase total bandwidth by channel bonding [11-13]. The present transceiver prototypes with a limited modulation index and low data rate complicate system

design with a four-phase subcarrier processor (SCP) and have poor reconfiguration [14]. The proposed regenerative transceiver architectures [15] with low power consumption have a tendency to be sensitive to circuit parameter variations and are considered not as robust as the conventional transceiver systems. The current transceiver implementation with relaxed subcarrier processor configuration and gated power control is not reflected for external mobile communication systems due to the lack of RF front-ends [16]. Another reconfigurable transmitter configuration [17] with a two-phase finite-module phase-locked loop was designed to targeting high data rate applications but encounters large subcarrier spurs as well as high power consumption. The transceiver designed in [18] with dual band-pass filters (BPFs) is difficult to make the BPF center frequency accurately tuned for wide frequency ranges.

In this paper, a reconfigurable transceiver for sub-6 GHz 5G wireless communication applications is designed and fabricated. With efficient RF front-end and external proposed MIMO antennas, the designed transceiver featuring low complexity and high robustness achieves a low bit error rate (BER) within the desired communication distance and accomplishes a low power consumption with a tenability property based on the IoT system platform. The designed transceiver applies a hybrid analog-digital beamforming architecture, which reduces the number of RF chains in MIMO systems. The designed transceiver uses a hybrid analog-digital beamforming architecture, which reduces the number of RF chains in MIMO systems, thus reducing power consumption [19-23]. Our proposed hybrid beamforming with 12-bit quantization has improved the energy efficiency by as high as approximately 100% over the conventional architectures with high-resolution A/D. A comparison of the introduced approach with the prior art is presented in Table 1. The organization of this manuscript is as follows. In Section II, the linearization of the energy-efficient power amplifier is presented and discussed. In Section III, a tunable filter controlled by IoT is proposed for the heterogenous sub-6 GHz 5G transceiver system. In Section IV, an eight-port and four-port MIMO array with

compact and dual-polarized slot-ring and radiators is designed and studied. The elements are deployed at the different edges of the mobile handset printed circuit board (PCB). In Section V, an RF agile transceiver using a highly integrated platform is discussed for the SECRET scenario. Section VI proposes the green and highly efficient RF transceiver including the fabricated prototype and system testing using MATLAB software. Finally, Section VII presents our conclusions.

Table 1
Comparison with Previous Works

	[9]	[10]	[11]	[12]	[13]	This Work
RF Frequency (GHz)	3.7-4.3	1.87-1.95	0.7-3.8	0.1-3.0	1.85-1.91	3.4-3.8
Beamforming Technique	Analog	Digital	Digital	Digital	Digital	Hybrid
Power Consumption (mW)	21-25	46	52	38-70	76	18-20
External Isolation (dB)	60	55	55	N/A	55	55
BER	10^{-6}	10^{-12}	N/A	N/A	N/A	$< 10^{-10}$
Modulation Scheme	2-FSK	BPSK	BPSK	BPSK	BPSK	64-QAM
Tunability	Yes	No	No	No	No	Yes
IoT Supported	No	No	No	No	No	Yes

II. Linearization of the power amplifier and energy efficiency for 5G

The main target of this use-case is to investigate, design and fabricate a fully compact, linearized and efficient active load modulation PA that can be used for 5G base stations, and to measure its performance.

A. General Description

The RF chain is a key block, responsible for high power consumption in mobile communications systems, where the PA is the main component responsible for consuming power: its main function is to boost the modulated signal without any distortion, and with the

highest possible efficiency. In the SECRET training program, the "efficiency enhancement technique" in the linear region of operation of PAs is being investigated. Several techniques are available, such as the use of Doherty power amplifiers (DPAs), Chireix out-phasing, envelope tracking (ET), envelope elimination and restoration (EER), and linear amplification using nonlinear components (LINC). Some of these techniques involve a complex architecture, external control circuits and signal processing, however, the Doherty configuration does not require any additional components, which together with its self-managing characteristics, makes its implementation attractive [24,25]. Accordingly, this use-case focuses on energy efficiency enhancement for RF PAs in the base station using the Doherty approach, linearizing the PAs by using Digital Pre-Distortion (DPD). The model is simulated with commercial software tools such as MWO and implemented on real hardware components that will be subjected to iterative optimization based on feedback from the simulation.

B. Problem Definition

The Doherty approach needs to be investigated in detail for the following reasons. The use-case aims to reduce the power consumption of RF PAs, "greening" the design. Modern modulated signals mainly rely on more complex modulation schemes, so that the modulated signal will have an envelope with a peak-average-power ratio (PAPR) that requires transmitters to be linear. However, linearity and power consumption are often conflicting aims in RF design. A PA can deliver its maximum efficiency near the saturation region; however, due to the use of a modulated signal that has PAPR, the amplifier needs to be backed-off from this most efficient region so that the required application linearity is obtained. In the back-off region, the amplifier efficiency drops sharply, where the unused DC power will be transformed into heat, requiring additional cooling and reducing the overall system efficiency.

C. Performance Metrics

Going beyond the state of the art, we have designed a compact Doherty amplifier with high efficiency. The design is shown in Figure 3 (a) and (b). It consists of two amplifiers, the main amplifier and the peaking amplifier, that work together to provide peak efficiency at the back-off output power while maintaining the required linearity. The two amplifiers are combined at point S, as shown in Figure 3 (a). The classical Doherty amplifier requires a quarter wavelength transmission line, whose main function is impedance inversion. In this modified design, a virtual impedance inverter was embedded in the design of the output matching network of the main amplifier, controlling both the impedance seen by the amplifier at the back-off point, and also the impedance seen when the peaking amplifier is working during load modulation. Thus, the challenge in designing this matching network is to provide the main amplifier with the exact impedances at both the back-off and the load modulation region. It should be noted that the central SMAs are used to test the designed Doherty power amplifier.

The main amplifier is active all the time, providing the overall efficiency since the system works most of the time in the back-off region where the peaking amplifier is off. The peaking amplifier is mainly responsible for injecting current into the summing point to increase the output power and to change the impedance seen by the main amplifier in the load modulation region [26]. The design of the peaking amplifier output matching network has two main targets, firstly is to provide a high impedance looking from the summing point (S) towards the peaking amplifier in the back-off region, and secondly to provide the peaking amplifier with an impedance that makes the amplifier generate its maximum power in the peak region of load-modulation when the peaking amplifier current is mainly responsible for determining the impedance modulation. Regarding the input matching network of both PAs, their main function is to control the achievable gain and gain flatness of each amplifier, and to ensure amplifier stability [27]. It should be noted that there are some interactions between the output matching

network and the input matching network which need to be taken into account. Furthermore, this study includes more PA designs that target different levels of output power with the highest efficiency and linearity. Some performance metrics may include power efficiency vs. linearity, dynamic range, bandwidth and suitable frequency tenability using IoT applications.

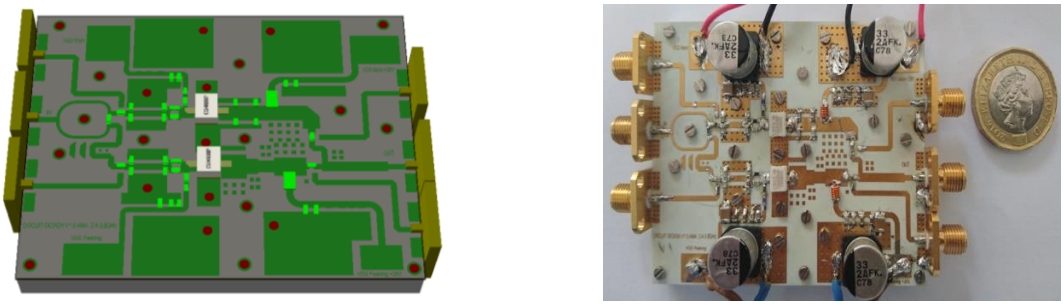

(a) (b)

Figure 3: The proposed amplifier (a) circuit layout (b) fabricated circuit.

The active load modulation amplifier was fabricated using a Roger RO4350B substrate with a thickness of 0.51 mm, targeting the sub-6 GHz band, with the amplifier working in the 3.4-3.8 GHz frequency band. The amplifier was able to deliver a gain of 11 dB with good gain flatness over the required band. The amplifier was also tested in terms of large-signal measurements using a Continuous-Wave (CW) signal. It can be seen from Figures 4 (a) and (b) that the amplifier was able to provide an average efficiency of 51% at 6 dB back-off from the peak power and an efficiency of 76% at the peak power of 41 dBm. In addition, the amplifier was also tested with a Wideband Code Division Multiple Access (WCDMA) modulated signal which has a PAPR of 7 dB at 35 dBm output power, where the amplifier linearity was tested with/without a digital pre-distortion (DPD). The linearity in terms of Adjacent Power Leakage Ratio ACLR was 30 dB without a lineariser, as shown in Figure 4 (c). By adding a 3rd generation RF PA lineariser (SC1894), the amplifier linearity was improved by 20 dB. Note that the load-modulation amplifier is very compact, efficient and linear which can be suitable for 5G base stations.

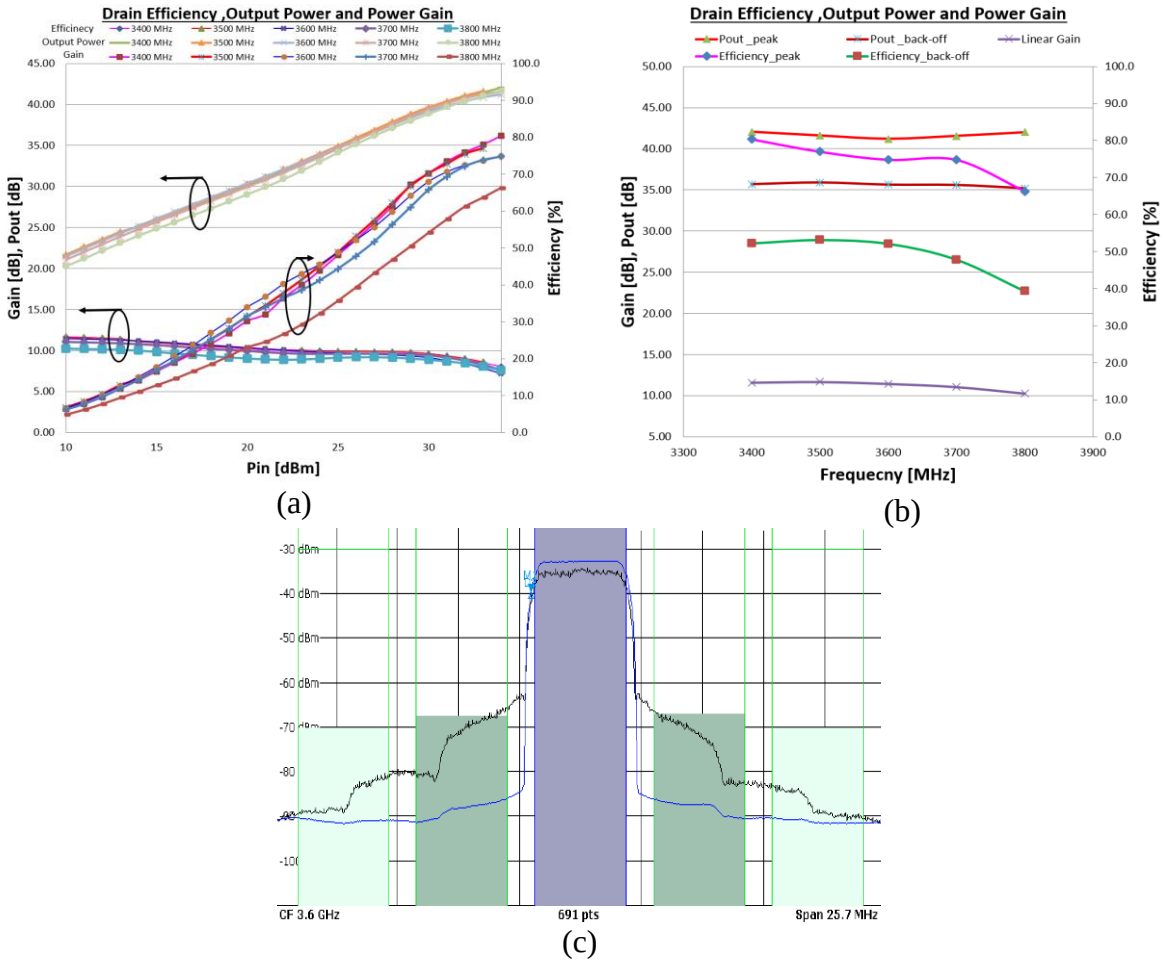

Figure 4: Measured load-modulation amplifier performance (a) CW-measurements vs. input power (b) CW-measurements vs. frequency (c) Amplifier linearity performance with/without DPD.

III. IoT controlled tunable filter

The objective of this part of the use-case is to model a compact tunable RF planar filter suitable for sub-6 GHz 5G applications with an emphasis on potential energy efficiency and good linearity. A compact planar tunable filter covering the 3.4-3.8 GHz spectrum for 5G wireless communications was designed, simulated, fabricated and measured.

A. General Description

Reconfigurable/tunable RF transceivers are increasingly studied for use in fifth-generation (5G) wireless applications [28]. To minimize the entire size of the communication

systems and construct a miniaturized RF front-end with high performance, several design techniques have been realized for reconfigurable components and many planar tunable filters have been presented [29, 30]. For example, Fu-Chang et al. [29] introduced a tunable dual-band band-pass planar filter utilizing two sets of half-wavelength resonators tuned by three PIN diodes and four varactor diodes. The structure was fabricated using Roger RO3010 substrate with a dielectric constant (ε_r) of 2.56, loss tangent of 0.003 and height (h) of 0.81 mm, giving the compact size of 35.8×34.5 mm^2. The operating frequency of the resonator was 2.42 GHz with an impedance bandwidth of about 45 MHz, with a resonant frequency tunable within the range 1.7-2.9 GHz (25.6% tuning range) using the seven diodes, with a return loss of more than 12 dB and insertion loss of less than 3.8 dB. Di et al. [30] presented a tunable dual/single-band planar filter using new synchronously adjusted dual-mode resonators and four Skyworks SMV1281-079LF varactor diodes. The roll-off skirt factor and out of band characteristics were developed by utilizing three finite transmission zeros. The filter had a stopband of up to 3.8 GHz of the resonant frequency. The tuned frequency covered 0.76-2.0 GHz with an adjustable impedance bandwidth within 73-160 MHz.

However, due to the rapid growth of recent wireless communications, compact and tunable/reconfigurable microstrip filter designs with low return loss and good stopband performance are required. Therefore, a tunable open-ended bandpass planar filter with good characteristics is proposed in this work for use in sub-6 GHz 5G wireless communications [31]. The filter uses three coupled line resonators with λ/4 open-circuited stubs and has a compact size of 13×8×0.81 mm^3. It is printed on a Rogers RO3010 substrate with a relative dielectric constant of 10.2 and is simulated and optimized using computer simulation technology (CST) software. Figure 5 (a) shows the geometry of the proposed filter, including the biasing circuit required to tune the varactor diodes, two choke inductors to prevent the RF signal from passing through the biasing circuit, and two DC block capacitors at each end of the design.

B. Problem Definition

It is intended that the future mobile handset will accommodate multiple standards, adopting reconfigurable handsets to reduce circuit duplication. This provides the impetus for a reconfigurable and tunable RF front-end structural design with metrics that include high energy efficiency, high tuning speed, excellent linearity, and low-loss or high-Q circuits. Varactor and MEMS technologies are seen as the most promising technologies. This use-case proposes to design and implement compact and highly selective tunable-switchable filter prototypes suitable for 5G technologies.

C. Performance Metrics

Going beyond the state of the art, we propose to design new tunable filters using varactor technology with emphasis on low-loss, low-power consumption, reduced size and high-Q, which would also allow easy integration with the antenna and Doherty power amplifier to implement the RF front-end. Frequency tunability is a desirable function for multi-band RF devices to tackle different wireless applications. Varactor diode switches are commonly used in planar filters to achieve tunable characteristics. Figure 5 (a) shows the configuration of the proposed tunable planar BPF with the electronic elements required to complete the biasing circuit. Two varactor diodes from Skyworks Inc (model SMV1234 and packaging size of 1.5 x 0.7 mm^2), two RF choke inductors (L = 10 nH) and two DC block capacitors (C = 10 pF) are used. To realize frequency tuneability, two parasitic transmission lines are implemented in parallel with the first and third resonators. The design parameters of these lines are selected and optimized with a length of 6 mm and a width of 1.4 mm for each: the gap between each line and the main resonating lines is 0.5 mm. CST software is used to obtain and optimize all the parameters. Among different varactor models, SMV1234 is applied here since it offers a wider capacitance range than others. Increasing the reverse biasing voltage (V_r) will widen the depletion region of the varactor so the capacitor values will be decreased and vice versa. Figure

5 (b) shows the obtained return and insertion losses for the tunable filter with different values of reverse biasing voltage, measured using an HP8510C vector network analyser. The diodes are biased using the same voltage source and controlled by using an IoT device NodeMcu, which is supported by the AD-FMC platform. As per the programmed software, the NodeMcu derives different voltage conditions across the varactor diodes, therefore, tuning the operating frequency bands. Instead of changing the voltage manually through cables, we used NodeMCU to control the PIN diodes remotely. Also, we can change the program and monitor it through the World Wide Web.

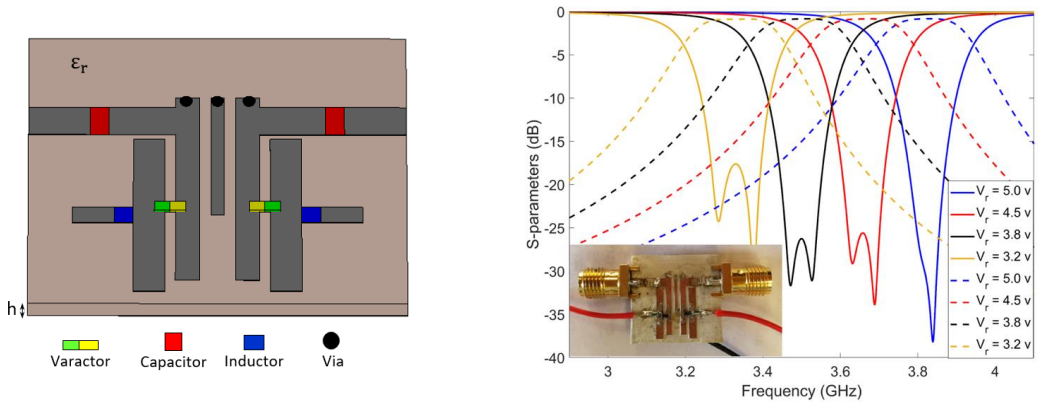

(a) (b)

Figure 5: The proposed tunable filter (a) configuration, (b) performance [solid line: return loss, dashed line: insertion loss], and a photograph of hardware realization.

It should be noted that increasing the reverse biasing voltages across the varactor diodes from 3.2-5.0 V will tune the centre frequency from 3.3-3.9 GHz with impedance bandwidth varying between 110-100 MHz. Also, less than 1 dB measured insertion losses and more than 18 dB return losses are obtained over the tuned S-parameters. The proposed design has some attractive properties, which include: (1) a compact and simple structure, (2) good stopband rejection and selectivity, and (3) the measured insertion loss is low with good return loss to cover the sub-6 GHz 5G (3.4-3.8 GHz) spectrum.

IV. MIMO Antennas for Multi-Mode Mobile Handsets

The main objective of this use-case is to design new antenna systems with polarization diversity and improved performance for sub-6 GHz 5G mobile handsets. The antennas have been fabricated, and their properties measured.

A. General Description

With the development of wireless communication systems, multiple-input/multiple-output (MIMO) techniques have been attracting attention for next-generation applications [32]. MIMO is a promising technology to enhance the performance of 5G networks. Although adding to the complexity of antenna design, it provides high data rates and improved spectral efficiency. In the case of massive MIMO, the 5G communication system also requires an array antenna with dual-polarization capability. MIMO antennas are proposed for use in smart and portable devices such as smartphones, laptops, etc. Among various types of MIMO antennas, microstrip antennas are more appropriate due to their attractive features, since they are small, light, and have low profiles. Moreover, microstrip antennas are easy to incorporate into practical applications to form a conformal antenna and they can be implemented to create multi-band antenna and multi-polarization antennas. In particular, microstrip antennas such as slot and monopole resonators are easy to integrate into a unified composition with active devices and microwave circuits, rendering them suitable for various applications [33].

B. Problem Definition

Unlike the millimetre-wave spectrum, sub-6 GHz 5G can provide wider coverage and fewer propagation losses. To support large amounts of high-speed data, at least 100 MHz impedance bandwidth should be supported. In comparison with 4G smartphones, six to ten elements are required to be integrated into handheld devices for 5G massive MIMO to achieve good diversity and multiplexing gain. Since the space of the smart device is limited, the

arrangement of multiple antennas with increased radiators is difficult, and the distances between antenna elements must be narrow. Thus, mutual coupling between array elements would be high without measures to reduce this serious problem. Several MIMO antennas have been introduced for sub-6 GHz 5G smartphone applications. However, all these antennas either occupy a large space or use non-planar, single-polarized radiators at different sides of PCB edges.

C. Performance Metrics

Going beyond the state of the art, we present an eight-port/four-radiator MIMO array with compact and dual-polarized slot-ring radiators. The single-element dual-polarized radiators are fed by independent microstrip lines that have been excited by coaxial-probe feedings. Unlike most reported 5G antennas, the proposed antenna simultaneously possesses anti-interference and polarization diversity characteristics [34]. The antenna elements are compact and operating at 3.6 GHz of the sub-6-GHz 5G band. The schematic is shown in Figure 6 (a). It has an overall size of 75×150 mm^2 and contains 8×8 ring-slot resonators with rectangular microstrip-line feedings with a size of 9.5×2 mm^2. It is designed on a 1.6 mm FR-4 substrate with a 4.3 permittivity and loss tangent of 0.002. The elements are deployed at the different edges of the mobile handset PCB. The inner and outer radii of the circular-ring slots are 7.7 and 8.85 mm, respectively. Employing dual-polarized slots not only improves the impedance-matching but also produces symmetrical radiation patterns covering the upper and lower regions of the smartphone PCB. The proposed design was fabricated and tested. The front view of the prototype sample is depicted in Figure 6 (b). Owning to similar characteristics of the antenna pairs, characteristics of the closely spaced antennas (Ant. 1 and Ant. 2) were measured and are discussed below. The measured and simulated S-parameter results (S_{nn} and S_{mn}) are plotted in Figures 6 (c) and (d): the slot elements exhibit well-defined S-parameters with sufficient frequency bandwidth and low mutual couplings, better than -15 dB.

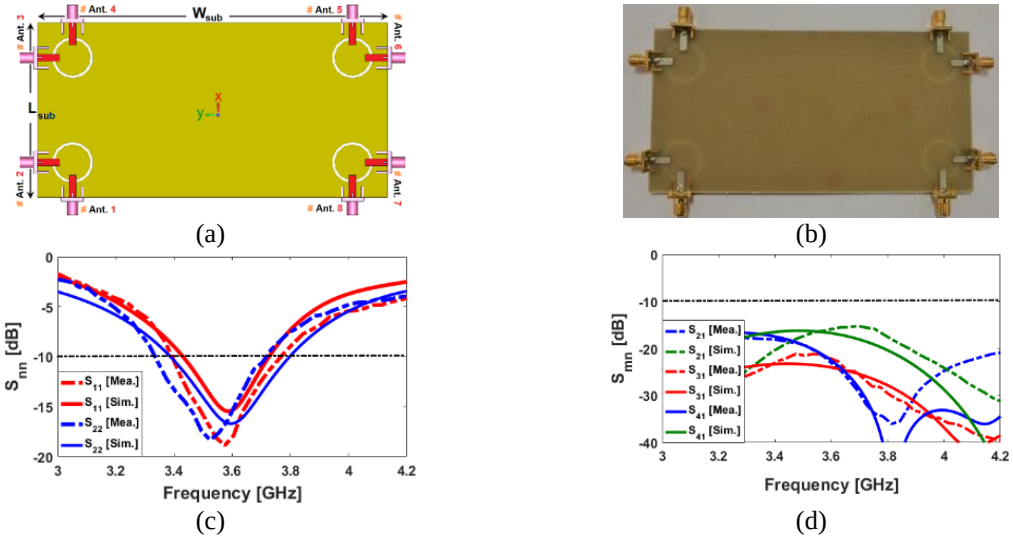

Figure 6: (a) Designed and (b) fabricated structures of the MIMO antenna; measured and simulated (c) reflection coefficient (S_{nn}) and (d) mutual coupling (S_{mn}) results.

3D transparent radiation patterns at 3.6 GHz for each slot resonator are shown in Figure 7 (a). It is observed that the dual-polarized ring slot elements not only cover different four sides of the smartphone mainboard but also support different polarizations (including vertical and horizontal) for each side of the board. Therefore, four horizontally and four vertically polarized radiations are available with this design, a unique feature that is due to the arrangement of the dual-polarized elements at four corner sides of the design and which can improve the MIMO performance of the system. In addition, it is found that the radiation elements offer reasonably good gain levels for each radiator at the desired operation frequency: as shown, the gain characteristic of each element is about 3-5 dB. The radiation and total efficiencies of the MIMO antenna system are also illustrated in Figure 7(b). Sufficient and well-defined efficiency results are obtained within the operation band of 3.4-3.8 GHz: more than 80% radiation efficiency is obtained for the antenna elements while total efficiencies varied around 65%-75%. The envelope correlation coefficient (ECC) is a critical parameter in MIMO antenna systems to indicate whether the system is effective [35]: this can be calculated from S-parameter results

and should be less than 0.5. Figure 7 (c) clearly shows that the calculated ECC results are well inside this threshold over the frequency band of the present design.

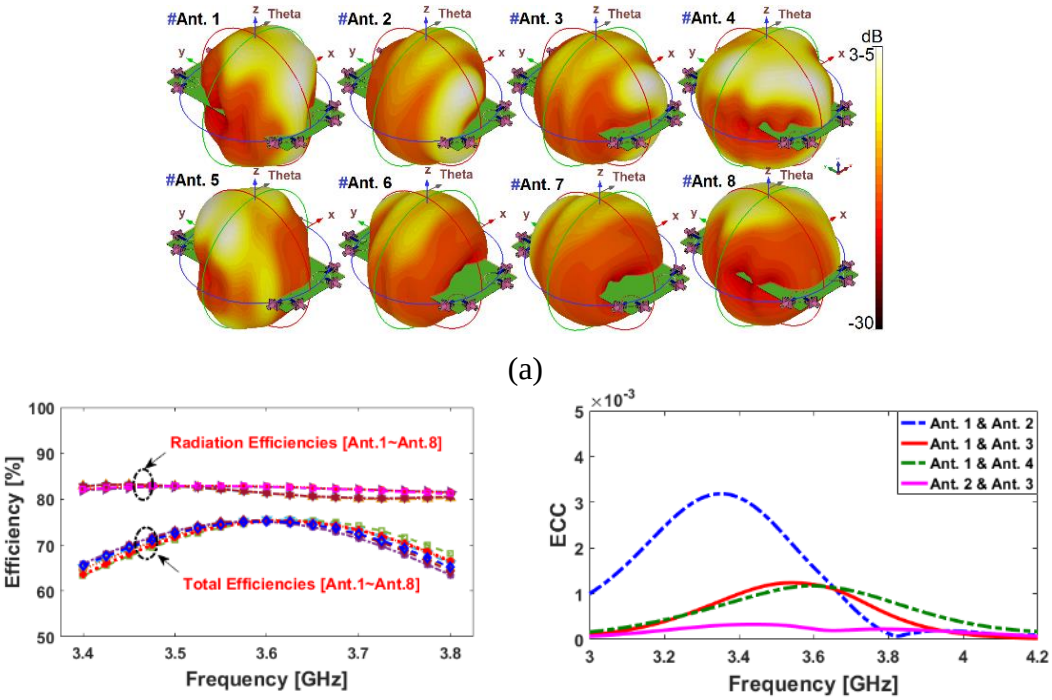

Figure 7: (a) 3D radiation patterns at 3.6 GHz, (b) radiation/total efficiencies of the elements and (c) the calculated ECC results of adjacent elements versus operation frequency.

Another approach for multi-mode function of the MIMO antennas is to support several frequency bands, simultaneously. It should be noted that apart from 3.6 GHz, some other frequencies such as 2.6 GHz and 5.2 GHz are considered to further support in sub 6 GHz 5G spectrum. In the following, another design of MIMO mobile-phone antenna array with multi-band function supporting 2.6, 3.6, and 5.2 GHz is introduced for higher data rate of 5G mobile applications. However, the frequency response and the radiation characteristic of the antenna are studied over the desired operating frequency band of 3.6 GHz (3.4 to 3.8 GHz). As shown in Figs 8 (a) and (b), its structure contains double-element square-ring slots fed by microstrip-lines placed at four corners of the mainboard with a standard size of 75×150 mm^2. Similar to the previous design, the introduced antenna array is arranged on an FR-4 material and provides sufficient scattering parameters and radiation properties. As depicted in Figs. 8 (c) and (d), for −10 dB impedance bandwidth, each element covers 3.4-3.8 GHz, LTE 42/43 of sub 6 GHz 5G applications. In addition, the mutual couplings of the antenna radiators exhibit less than -25 dB at the operational band.

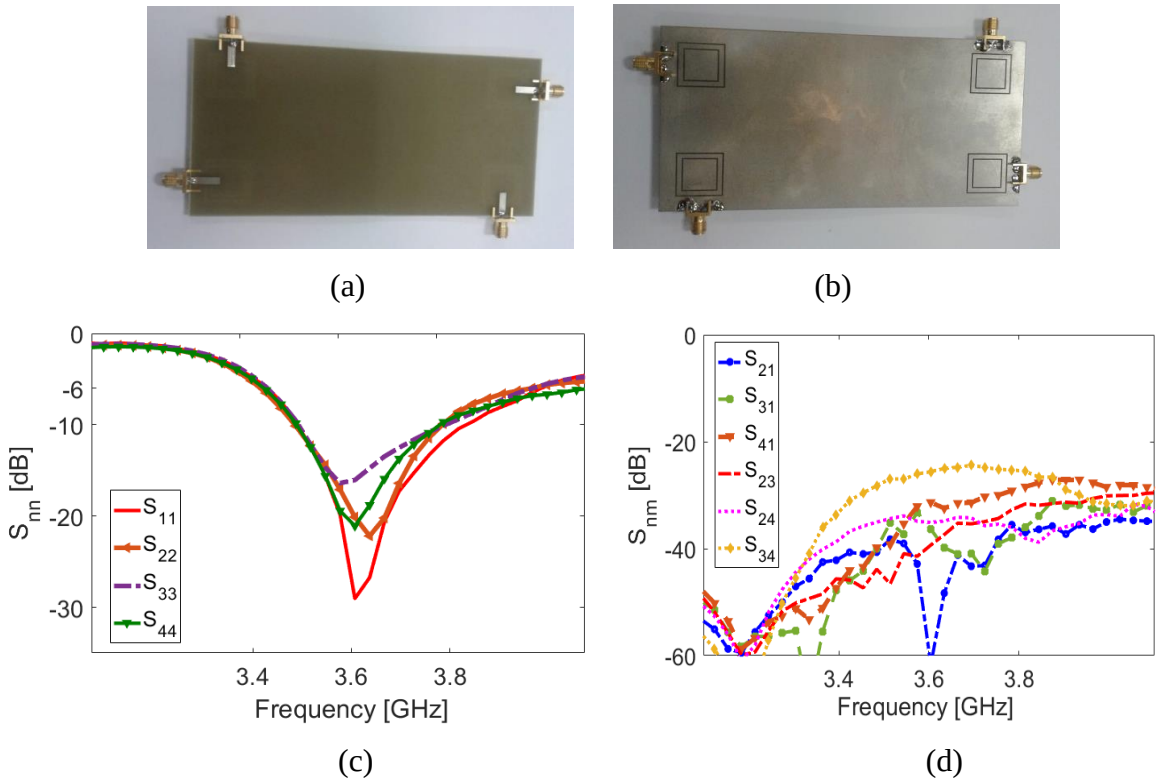

Figure 8: Antenna performance (a) Front and (b) back views of the fabricated prototype and its measured (c) Snn, and (d) Smn results.

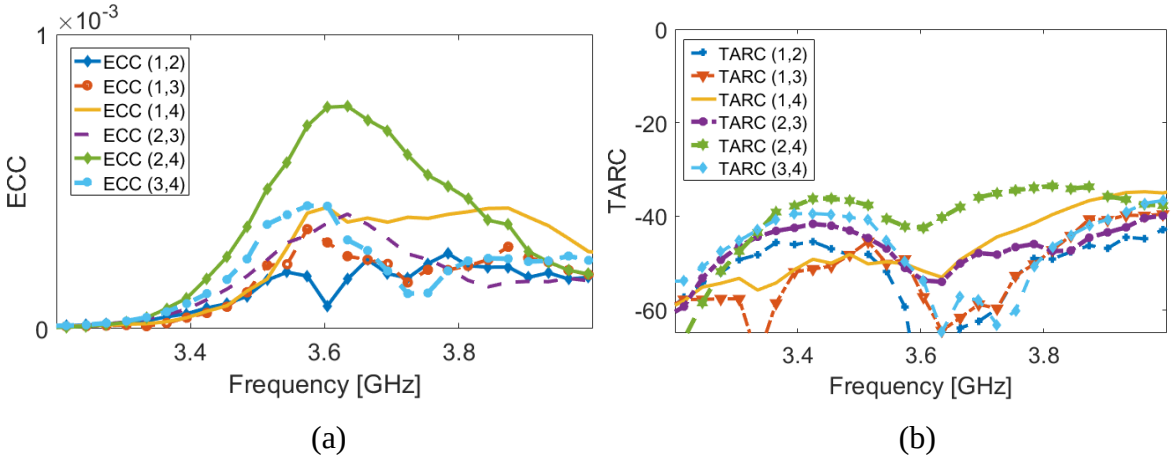

Figure 9: Antenna performance (a) ECC and (b) TARC results.

Apart from the antenna S-parameters, other specifications such as envelope correlation coefficient (ECC) and the total active reflection coefficient (TARC) are critical parameters in MIMO systems. The ECC quantifying multiple-port performance of the antenna system while TARC is defined as the square root of the ratio of reflected power. A lower ECC means more diversified patterns. Therefore, according to the requirements, in order to have a better MIMO performance, the ECC and TARC results of an antenna system should be in low levels. Figures 9 (a) and (b) represent the ECC and TARC results of the closely spaced elements. It is seen

that the ECC and TARC functions of the introduced MIMO array are very low within 3.4-3.8 GHz. The 3D radiation patterns with and without linear scaling for each element at 3.6 GHz are illustrated in Figs. 10 (a) and (b). It is clear that each side of the smartphone mainboard can be covered by the radiations of the elements. This is due to proper placements of the antenna feed lines which can improve the performance of the antenna system by providing full radiation coverage. In addition, sufficient gain values are observed at the target frequency (3.6 GHz).

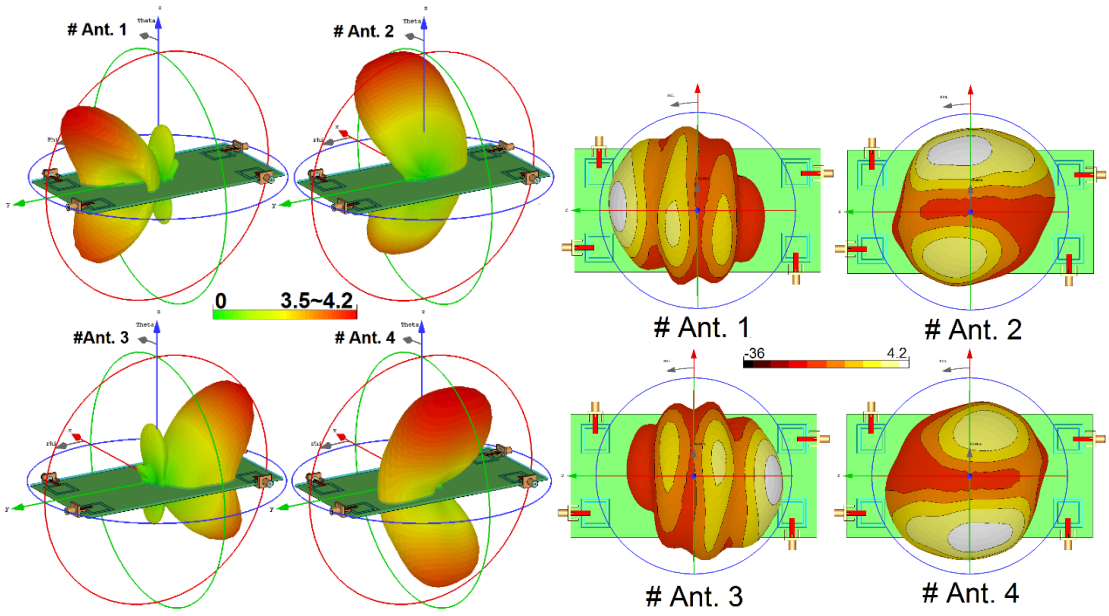

(a) (b)

Figure 10: Radiation patterns of the antenna elements (a) with and (b) without linear scaling.

V. RF front-end system

Figure 11 shows a block diagram of the suggested transceiver for the SECRET scenario. The transmitter/receiver consists of the AD-FMCOMMS5-EBZ (AD-FMC) through the ZC706 Xilinx IoT-controlled platform integrated with the front-end components, namely, Doherty PAs, tunable filters and MIMO antennas. The AD-FMC is a high-speed analog module designed to showcase the AD9361 in MIMO applications. We preferred to extract the scattering parameters of the power amplifier (explained in Section II), then include these parameters inside the software and hardware of the AD-FMC, to reduce the possibility of interfering with other users, because the spectrum we are working on is not free license. For

the tunable filter, and to reduce the complexity and the size of the implemented system, we have considered only one prototype design and employed the prototype of Section III, while fixed the other filters (with the same performance and equivalent characteristic equation) which are already embedded inside the AD9361 platform (as shown in Figure 12). The system is prototyped to prove the concept of the SECRET scenario as recommended by our industry partner. Of course, we will need 4 tunable filters and 4 PAs at each side of the channel in a realistic model. For simplicity, a 4×4 MIMO smartphone antenna described in Section IV has been integrated with this system. It should be noted that the 8-element antenna can be also used instead. In this case, 50-Ohm loads must be applied for the elements which are not under test.

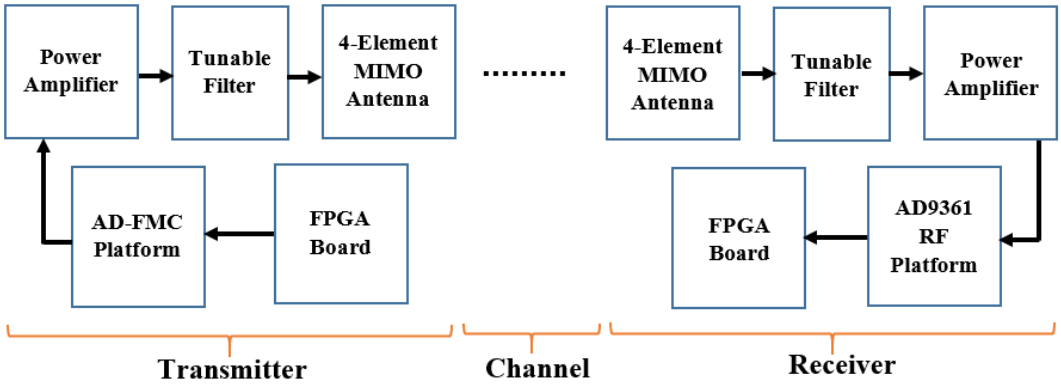

Figure 11: Block diagram for the suggested system.

A. RF-Agile Transceiver

The AD9361 is an efficient, widely adopted RF Agile transmitter/receiver employed in 4G and 5G mobile handset and base station systems. Figure 12 shows the block diagram of the AD9361 communication system [36]. Its programmability and wideband operation performance make the device an excellent option for wide-ranging wireless front-end communications. The device incorporates a transceiver with adaptable different baseband signal parts and combined frequency synthesizers, reducing the complexity by offering a configurable digital interface to a processor. The AD9361 transmitting chain local oscillator works from 47 MHz to 6.0 GHz and the transmitting chain local oscillator works from 70 MHz to 6.0 GHz ranges, operating on several licensed and unlicensed spectrum with an operating

bandwidth from < 200 kHz to 56 MHz can be obtained. The two isolated direct conversion receiving ends have state-of-the-art noise figure and linearity. The receiver sub-system contains separate automatic gain control (AGC), DC-offset control, quadrature control, and digital filtering tool, in a manner to avoid these required elements in the digital baseband.

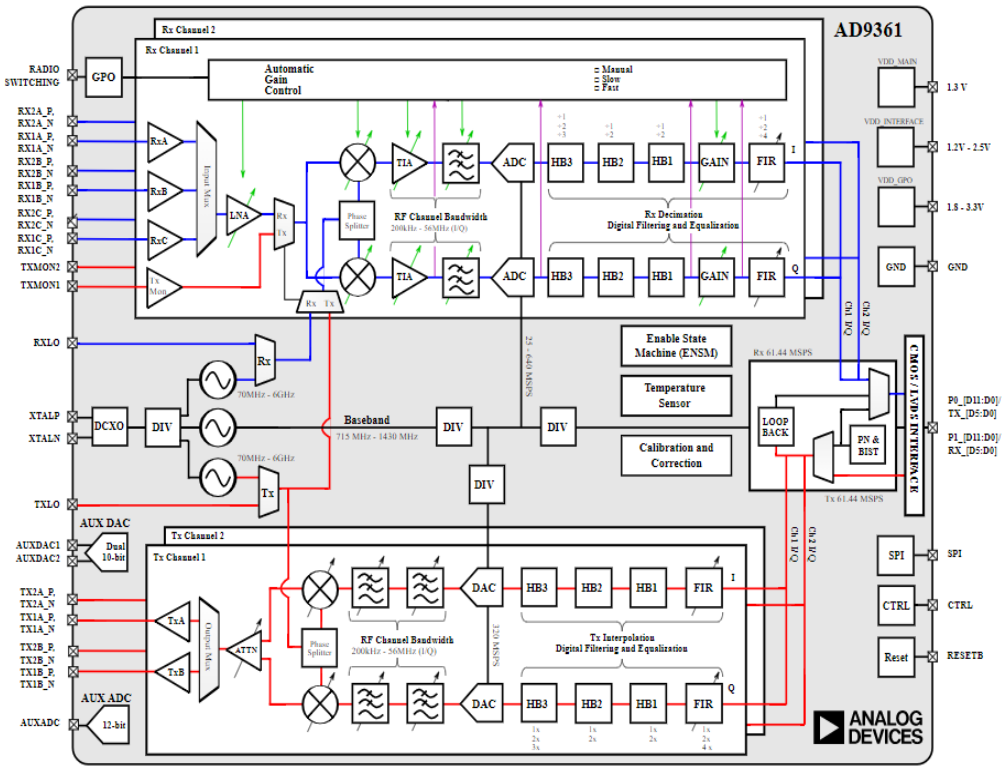

Figure 12: The block diagram of the AD9361 transceiver [36].

B. Transmitter

The transmitter side includes two similar and separately adjusted channels that deliver all digital processing, mixed-signal, and RF platforms required to achieve a direct conversion function while providing a common frequency synthesizer. The transmitting signal pathway has 12-bit 2s complement data in I-Q layout from the digital interface, and each channel (in-phase (I) and quadrature (Q)) passes this data through a fully programmed 128-tap finite impulse response filter with interpolation selections. The finite impulse response filter output is provided to a series of several other filters that deliver extra filtering and data rate interpolation before realizing the 12-bit digital to analogue converter (D/A). The finite impulse

response filter and the additional filters can separately be managed and bypassed when required. Each 12-bit D/A has a controllable sampling rate. The D/A converter's analogue output is passed through two lowpass filters before the RF mixer. The corner frequency for each lowpass filter can also be programmed. At this instant, the I-Q signals are re-integrated and modulated on the carrier frequency to be transmitted to the output terminal. The integrated signal also passes through analogue filters to improve the transmission selectivity, and then to the output power amplifier. The transmitting channel delivers a wide attenuation amendment range with fine granularity to enable engineers to obtain an optimized signal-to-noise ratio.

C. Receiver

The receiver side consists of all components required to receive RF signals and convert them to a digital signal. Two separately controlled channels can receive data from different terminals, making the system able to be utilized in multi-input, multi-output communications while sharing a common frequency synthesizer. The channel has three inputs that can be multiplexed to the signal chain, allowing the AD9361 device to be applicable for diversity/MIMO antenna systems. The receiver is a direct conversion system that consists of a low noise power amplifier, I and Q matching amplifiers, mixers, and bandpass filtering elements that down-convert received signals to baseband for digitization. Additional low noise power amplifiers can also be added to the circuit, providing the designers with a more flexible tool to modify receiver front-ends for their targeted applications.

D. Rx and Tx Filtering

In both the transmitter and receiver sides, there are:

- Digital interpolation/decimation filters to up/down convert from the digital baseband rate (64.11MSPS max) to the real analogue to digital conversion 640MSPS or 320MSPS rates.

- Analogue lowpass filters either to eliminate sampling artefacts on the transmit chain or to the band forming to minimize adjacent channel interference on the receive chain.

Analogue or digital design for these filters does not affect the magnitude and phase in the passband signals because this should be recompensed somewhere in the RF platform. It can simply be accomplished inside the 128-tap finite impulse response. The finite impulse response filter is not only utilized to serve as a low pass filter but also to recompense for the magnitude and phase affects the analogue and digital half-band filters created in the baseband window of interest. Figure 13 illustrates the performance of the filters designed in the AD9361 transceiver device. The four filters decimate by at least 2, so their pass-bands extend over nearly the total output bandwidth of the finite impulse response filter. Because these filters do not affect the performance of the upstream half-bands, D/A, and analogue filters, the entire amplitude performance of the front-end device can tapper as these filters are set with less bandwidth.

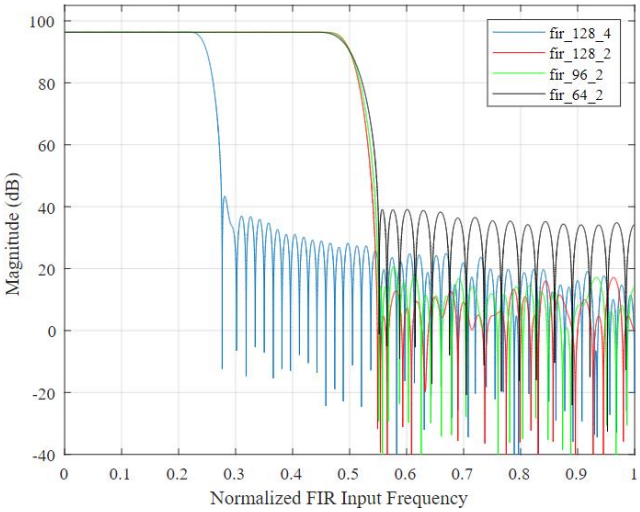

Figure 13: Rx and Tx Filter response.

E. System implementation and measurements

In this subsection, we aim to test the system performance by integrating the previously implemented RF elements with the ZC706 FPGA and AD-FMC platforms. Figure 12 shows the suggested block diagram for the system and the implemented system including the elements presented above, respectively. As illustrated in Figure 14 (a), a baseband signal can be

generated easily using either MATLAB code or Simulink blocks. The generated baseband signals can be processed to be sent through the antennas of AD-FMC through the Xilinx platform (ZC706). LTE Toolbox is used to generate the uplink and downlink reference measurement channel (RMC) waveforms by defining the RMC configurations, identifying the cell and determining the number of frames that will be sent after specifying the operating frequency and the number of using antennas. In order to test the system, an image will be sent through it. The image is converted into a binary stream, fed to input of the LTE toolbox to generate the baseband waveform depending on the selected standards. After that, the generated baseband waveforms are fed to the AD-FMC through the ZC706 platform, where the signal is modulated using 64-QAM and carried at a carrier frequency of 3.7 GHz.

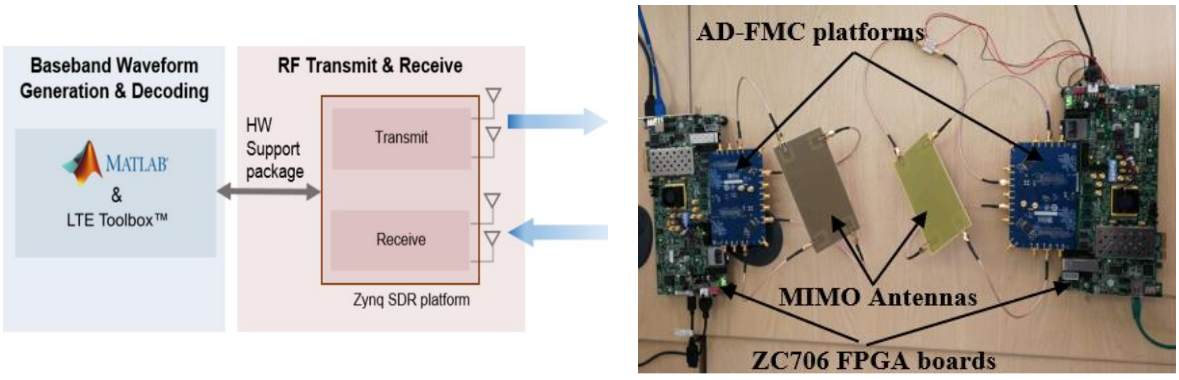

(a) (b)

Figure 14: The proposed system (a) A conceptual overview. (b) Implemented hardware.

The carrier frequency can be easily modified using the programme code across a wide frequency range of 70 MHz to 6.0 GHz. The RF output signal is transmitted using four different antennas at the transmitting side and also four antennas are used for the receiving (4×4). At the receive side, the AD-FMC is programmed to operate at the transmitted frequency, where the RF signal goes through LNA, filters and A/D blocks to generate the I/Q baseband waveforms, where the frequency offset is determined and corrected. In addition, the LTE frame is synchronized so that the OFDM demodulation can be performed where data decoding process is necessary to recombine the data to form the received signal.

At the same time, channel estimation for the received signal is performed using cell-specific reference signals, where an averaging window is used to minimize the noise effect. As shown in Figure 15, various MIMO orientations were considered for measurements with and with hand-free and almost similar results are achieved. The antenna orientation is studied in two different scenarios including face to face and side by side This could be due to the symmetrical configuration of the antenna system with stability function at different setups. The impact of the user-hand was not significant during the measurement, since the antenna provides sufficient performance in the presence of the user-hand. The proposed method is also very flexible and can be repeated and extended to higher MIMO orders. It was observed that the BERs over all these different scenarios were consistent, as reported in Table 1. Moreover, various bandwidth spectrums such as 5, 10, 20 and 30 MHz have also been tested to handle the MIMO communication links and the results were quite satisfactory in terms of achieving the required BER. Moreover, the MIMO handsets over many distances within our test lab (lab size: 8 x 14 x 3.6 m^3) have been tested, in which we are able to investigate the transmitted data for a line of sight and non-line of sight for many positions and locations. We have also included the concept of LOS and NLOS when a user sits in between, the achievable BER was found between 10^{-8} and 10^{-10} for a maximum output power of 1.5, 4.5 and 7.5 dBm (the lower power was adjusted by integrating 3dB attenuators within the transmitted power of the MIMO handset). In general, we aimed by this test to confirm the radiation diversity of our new MIMO system. Figure 16, summarizes the variations of the BER based on all possible MIMO handset orientations. It is clear the radiation pattern diversity of the proposed MIMO handset was approved over the range of the output power considered here.

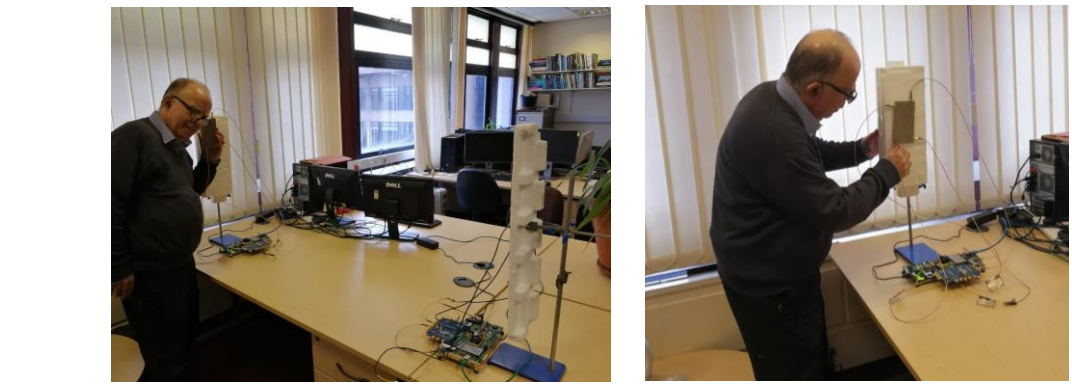

(a)

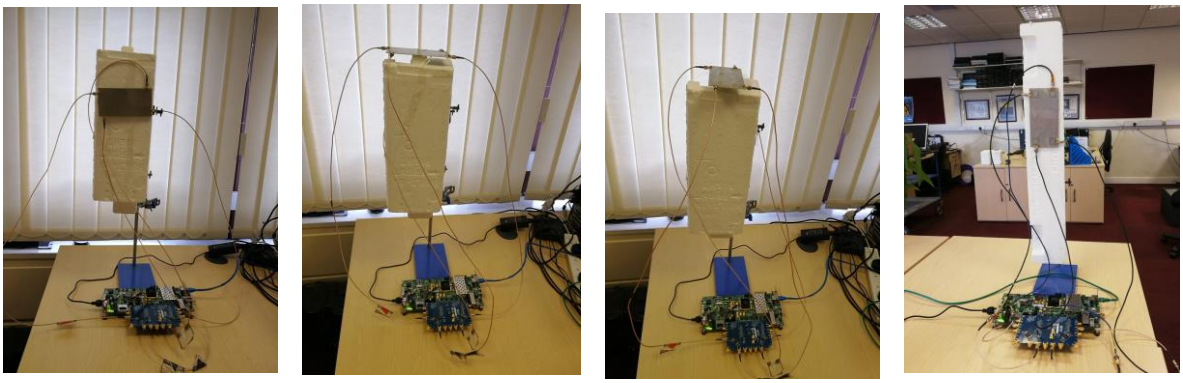

(b)

Figure 15: Various MIMO handset orientations with (a) hand, (b) hands-free.

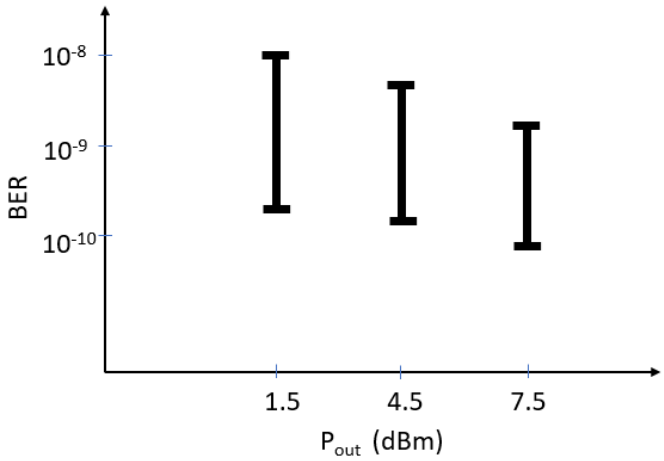

Figure 16: System performance with different scenarios.

There was a very high correlation between the transmitted and received data with a reliability of more than 99% (based on the image size and BER). At the same time, the system stability, repeatability and consistency were very high. Figure 17 shows the received baseband

spectrum of the four received signals that come from the four antennas, it can be seen from the figure that all receive channels are performing well, where the signal bandwidth is 10 MHz. The performed channel estimation is shown in Figure 18 where the channel information is plotted for each subcarrier and symbols indexes.

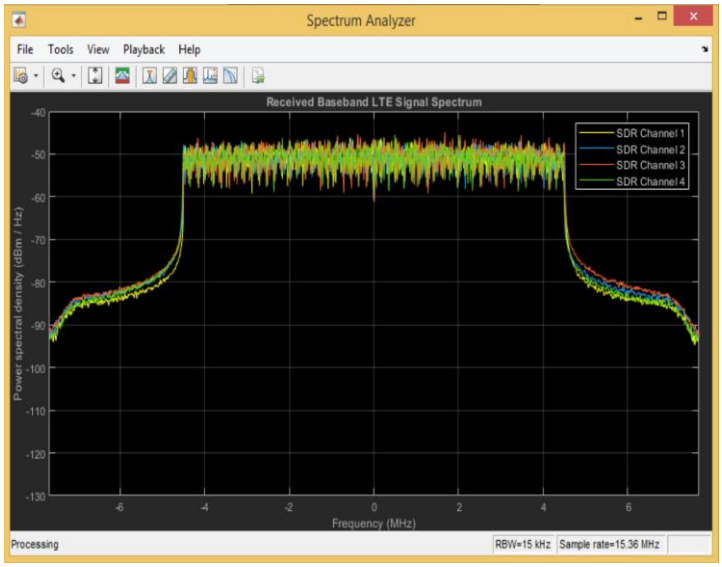

Figure 17: The spectrum of the received signals from four antennas.

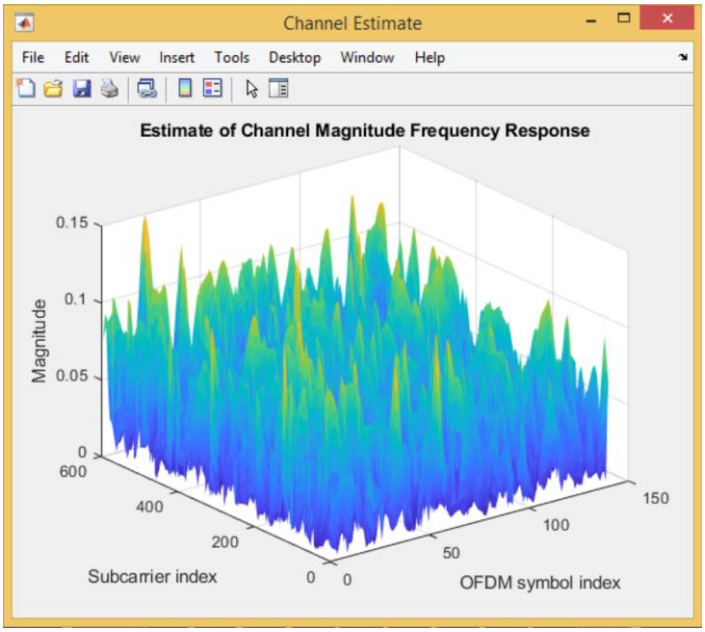

Figure 18: Channel estimation response.

A constellation diagram of the equalized received symbols is shown in Figure 19, where a normalized 64-QAM constellation of the received symbols is plotted. After demodulating the received symbols to form the received data, the obtained image is shown in Figure 20. It is

worthy to mention that the standard MIMO smartphone antenna systems tend to use two or four antenna elements in a single physical profile. While massive MIMO employs an especially high number of antennas which can improve the performance of the system and make it more resistant to interference and jamming. In cellular communications, this task is attained by incorporating multiple antenna elements (six to ten) into the limited space of the smartphone board which is advantageous for 5G practical applications [37].

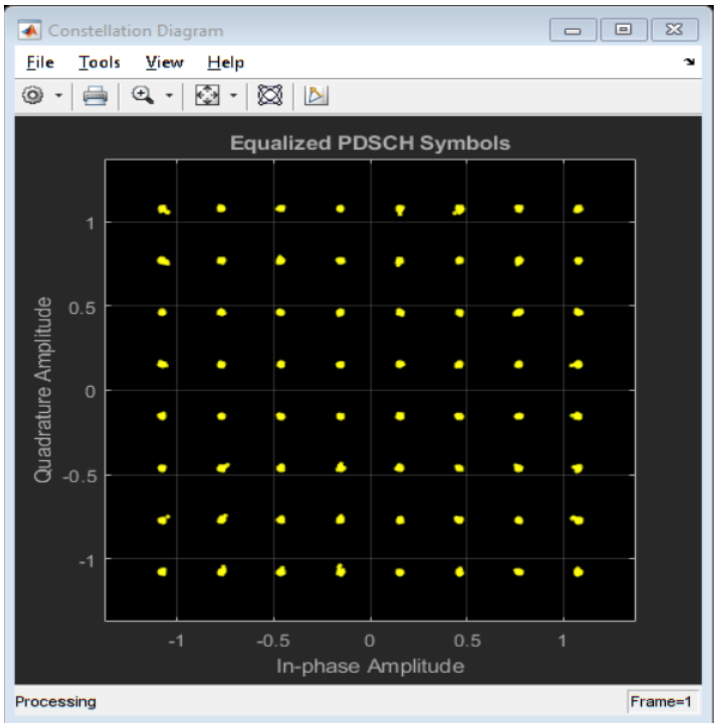

Figure 19: Constellation of the received symbols.

Figure 20: The received image compared with the transmitted one.

VI. Conclusion

A green RF front-end is proposed within the SECRET project for integration on a single layout circuit model for future emerging 5G transceivers, where a highly efficient amplifier, compact filter and MIMO antennas are used. The designed amplifier is used to increase the efficiency of the system, whereas increasing the number of transmitting and receiving antennas enhances the overall system capacity. The system channel is tunable and controllable using the IoT filtering platform. The design is built on RF standardization and spectrum policy requirements and engineered to provide minimal power consumption of 18-20 mW. The design procedures were applied towards optimising the RF chain parameters of future 5G devices and to establish the limits and the constraints, especially in terms of effective consumed power for heterogenous transceiver systems. Furthermore, a MIMO transceiver using AD-FMC through

the ZC706 platform was designed and programmed, where a MATLAB code was employed to transmit and receive a picture using four antenna elements. The practical system was able to send and receive the picture correctly after specifying the operating frequency and the bandwidth for each channel. The generated baseband waveforms were fed to the communication platform, where the signal is modulated using 64-QAM and carried at a carrier frequency of 3.6 GHz. The system has achieved a BER of less than 10^{-10} at a data rate of 600 Mb/s with a wireless communication distance of more than 1 meter and low power dissipation by employing hybrid beamforming technology. Using the three-way Doherty amplifier, the system was able to achieve a peak power of 48 dBm with more than 75 % efficiency at the peak power.

Acknowledgments

This work is supported by the European Union's Horizon 2020 Research and Innovation program under grant agreement H2020-MSCA-ITN-2016-SECRET-722424.

References

[1] A. Gupta, R. Kumar, "A Survey of 5G Network: Architecture and emerging technologies," IEEE Access, vol. 3, July 2015, pp. 1206-1232.

[2] B. Hammond, "New System Design Tools for 5G RF Front- Ends," Microwaves and RF Magazine, January, 2017.

[3] Flex5Gware, "WP 2 – RF front-ends and antennas; D 2.1 Requirements and concepts for the analogueue HW in 5G mobile systems," December, 2015.

[4] Nokia white paper, "5G Radio Access System Design Aspects," 2017.

[5] D. Pehlke, D. Brunel, K. Walsh, S. Kovacic, "Sub-6GHz 5G for UE, Optimizing cell edge user experience," IWPC 4G/5G Multi-band, Multi- Mode User Equipment, Austin, October 2017.

[6] GTI, Sub-6GHz 5G Device, White Paper, Nov. 2017.

[7] Statement: Improving Consumer Access to Mobile Services at 3.6 GHz to 3.8 GHz. Available online: https://www.ofcom.org.uk/consultations-and-statements/category-1/future-use-at-3.6-3.8-ghz (accessed on 21 October 2018).

[8] J. Rodriguez *et al*., "SECRET — Secure network coding for reduced energy next generation mobile small cells: A European Training Network in wireless communications and networking for 5G," *2017 Internet Technologies and Applications (ITA)*, Wrexham, 2017, pp. 329-333.

[9] B. Zhou, F. Chen, W. Rhee and Z. Wang, "A Reconfigurable FM-UWB Transceiver for Short-Range Wireless Communications," in IEEE Microwave and Wireless Components Letters, vol. 23, no. 7, pp. 371-373, July 2013.

[10] K. Lee and J. Sim, "Half-Rate Clock-Embedded Source Synchronous Transceivers in 130-nm CMOS," in IEEE Transactions on Very Large Scale Integration (VLSI) Systems, vol. 22, no. 10, pp. 2093-2102, Oct. 2014.

[11] S. Sadjina et al., "A mixed-signal circuit technique for cancellation of interferers modulated by LO phase-noise in 4G/5G CA transceivers," IEEE Trans. Circuits Syst. I, Reg. Papers, vol. 65, no. 11, pp. 3745–3755, Nov. 2018.

[12] D. Murphy, H. Darabi, and H. Xu, "A noise-cancelling receiver resilient to large harmonic blockers," IEEE J. Solid-State Circuits, vol. 50, no. 6, pp. 1336–1350, Jun. 2015.

[13] A. Elmaghraby et al., "A mixed-signal technique for TX-induced modulated spur cancellation in LTE-CA receivers," IEEE Trans. Circuits Syst. I, Reg. Papers, vol. 65, no. 9, pp. 3060–3073, Sep. 2018.

[14] J. F. M. Gerrits et al., "A 7.2 GHz–7.7 GHz FM-UWB transceiver prototype," in Proc. IEEE ICUWB, Sep. 2009, pp. 580–585.

[15] N. Saputra and J. R. Long, "A short-range low data-rate regenerative FM-UWB receiver," IEEE Trans. Microw. Theory Tech., vol. 59, no. 4, pp. 1131–1140, Apr. 2011.

[16] B. Zhou et al., "A gated FM-UWB system with data-driven front-end power control," IEEE Trans. Circuits Syst. I, vol. 59, no. 6, pp. 1348–1358, Jun. 2012.

[17] B. Zhou et al., "A 1 Mb/s 3.2–4.4 GHz reconfigurable FM-UWB transmitter in 0.18 CMOS," in Proc. IEEE RFIC, Jun. 2011, pp. 1–4.

[18] F. Chen et al., "A 3.8 mW, 3.5–4 GHz regenerative FM-UWB receiver with enhanced linearity by utilizing a wideband LNA and dual bandpass filters," in Proc. IEEE RFIT, Nov. 2012, pp. 150–152.

[19] V. N. Ha, D. H. N. Nguyen and J. -F. Frigon, "System Energy-Efficient Hybrid Beamforming for mmWave Multi-User Systems," in IEEE Transactions on Green Communications and Networking, vol. 4, no. 4, pp. 1010-1023, Dec. 2020.

[20] M. Sefunç, A. Zappone and E. A. Jorswieck, "Energy Efficiency of mmWave MIMO Systems With Spatial Modulation and Hybrid Beamforming," in IEEE Transactions on Green Communications and Networking, vol. 4, no. 1, pp. 95-108, March 2020.

[21] A. Kaushik, J. Thompson, E. Vlachos, C. Tsinos and S. Chatzinotas, "Dynamic RF Chain Selection for Energy Efficient and Low Complexity Hybrid Beamforming in Millimeter Wave MIMO Systems," in IEEE Transactions on Green Communications and Networking, vol. 3, no. 4, pp. 886-900, Dec. 2019.

[22] X. Song, S. Haghighatshoar and G. Caire, "Efficient Beam Alignment for Millimeter Wave Single-Carrier Systems With Hybrid MIMO Transceivers," in IEEE Transactions on Wireless Communications, vol. 18, no. 3, pp. 1518-1533, March 2019.

[23] L. Yang, Y. Zeng and R. Zhang, "Wireless Power Transfer With Hybrid Beamforming: How Many RF Chains Do We Need?," in IEEE Transactions on Wireless Communications, vol. 17, no. 10, pp. 6972-6984, Oct. 2018.

[24] Y. Xu, J. Pang, X. Wang and A. Zhu, "Enhancing Bandwidth and Back-Off Range of Doherty Power Amplifier With Modified Load Modulation Network," in *IEEE Transactions on Microwave Theory and Techniques*, vol. 69, no. 4, pp. 2291-2303, April 2021.

[25] H. Kang, W. Choi, I. Kim, D. Lee and Y. Yang, "500 W Three-way GaN Doherty Power Amplifier for Sub-6 GHz 5G New Radio Base Transceiver Systems," *2020 50th European Microwave Conference (EuMC)*, Utrecht, Netherlands, 2021, pp. 312-315.

[26] A. M. Abdulkhaleq et al., "Load-Modulation Technique Without Using Quarter-Wavelength Transmission Line," IET Microwaves, Antennas & Propagation, 2020.

[27] A. M. Abdulkhaleq et al., "A Compact Load-Modulation Amplifier for Improved Efficiency Next Generation Mobile," Accepted at the 50th The European Microwave Conference (EuMC), The Jaarbeurs, The Netherlands, 2020.

[28] A. A. Boulogeorgos and A. Alexiou, "Performance Analysis of Reconfigurable Intelligent Surface-Assisted Wireless Systems and Comparison With Relaying," IEEE Access, vol. 8, pp. 94463-94483, 2020.

[29] F. Chen, R. Li and J. Chen, "A Tunable Dual-Band Bandpass-to-Bandstop Filter Using p-i-n Diodes and Varactors," IEEE Access, vol. 6, pp. 46058-46065, 2018.

[30] D. Lu, X. Tang, N. S. Barker and Y. Feng, "Single-Band and Switchable Dual-/Single-Band Tunable BPFs With Predefined Tuning Range, Bandwidth, and Selectivity," IEEE Transactions on Microwave Theory and Techniques, vol. 66, no. 3, pp. 1215-1227, March 2018.

[31] Y. I. A. Al-Yasir et al., "A Varactor-Based Very Compact Tunable Filter with Wide Tuning Range for 4G and Sub-6 GHz 5G Communications," Sensors, vol. 20, no. 16, p. 4538, 2020.

[32] Q. Nadeem, et al., “Design of 5G full dimension massive MIMO systems,” IEEE Trans. Commun., vol. 66, pp. 726–740, 2018.

[33] C. A. Balanis, “Antenna theory analysis and design-4th edition,” John Wiley & Sons, New York, 1998.

[34] M.S. Sharawi, “Printed multi-band MIMO antenna systems and their performance metrics [wireless corner],” IEEE Antennas Propag. Mag. vol. 55, pp. 218–232, 2013.

[35] N. Ojaroudi Parchin, Y. I. A. Al-Yasir, H. Jahanbakhsh Basherlou, R. A. Abd-Alhameed and J. M. Noras, "Orthogonally dual-polarised MIMO antenna array with pattern diversity for use in 5G smartphones," in *IET Microwaves, Antennas & Propagation*, vol. 14, no. 6, pp. 457-467, 20 5 2020.

[36] https://www.analogue.com/en/index.html

[37] M. Temiz, E. Alsusa, L. Danoon and Y. Zhang, "On the Impact of Antenna Array Geometry on Indoor Wideband Massive MIMO Networks," in *IEEE Transactions on Antennas and Propagation*, vol. 69, no. 1, pp. 406-416, Jan. 2021.

 **Yasir Al-Yasir** (Member, IEEE) is currently a Staff Member at the Faculty of Engineering and Informatics, University of Bradford, working as a Research Fellow in the SATNEX-V project, funded by the European Space Agency. He received the B.Sc. and M.Sc. degrees from the University of Basrah, Iraq, in 2012 and 2015, respectively, and the Ph.D. degree from the University of Bradford, U.K., in 2021. In 2014, he joined the Antennas and RF Engineering research group as a research visitor at the University of Bradford. From 2018 to 2020, he was appointed at the University of Bradford as a Marie Curie Research Fellow in the H2020-ITN-SECRET project funded by EU Commission, targeting 5G mobile small cells. He is also a Reviewer for various high-ranking journals and publishers such as IEEE, IET, Wiley, Springer, Elsevier, and MDPI. Dr Al-Yasir is the recipient and a co-recipient of various awards and prizes such as the Best Paper Award at the IEEE 2nd 5G World Forum and IEEE 4th 5G Summit Dresden, Germany. He has authored 2 books and 10 book chapters and published more than 130 journal and conference papers on aspects of RF and Microwave Engineering. His articles have more than 1500 citations with 22 h-index, reported by the Google Scholar.

 **Ahmed Abdulkhaleq** (Member, IEEE) was born in Mosul, Iraq, in 1988, he received his BSc in Communications Engineering with a first-class ranking from University of Mosul, Iraq in 2009. In 2010-2011, he worked as an engineer at the college of Electronics, University of Mosul, Iraq. In 2011-2013, he received a scholarship from the Higher Committee for Education Development in Iraq (HCED-Iraq) to complete his master's degree. In 2013, he was awarded the MSc degree with distinction from the University of Bradford, UK. In 2013-2017, he worked as a lecturer at University of Nineveh, Iraq. in 2018-2020, Ahmed appointed as an Early-Stage Researcher in Secure Network Coding for Reduced Energy Next Generation Mobile Small Cells (SECRET) project. this project is part of the Horizon 2020 Marie Sklodowska-Curie Actions funded by the European Union. In 2020, he received the PhD degree from the University of Bradford, UK. Currently he is an RF/Microwave Engineer at SARAS technology in Leeds, UK. He is an author and co-author of many international journal and conference papers. His research interests include energy-efficient RF power amplifiers, Digital Signal Processing (DSP), filters, antenna array processing and reconfigurable transceivers. He was also a recipient and a co-recipient of various awards for research publications.

 **Naser Ojaroudi Parchin** (Member, IEEE) received the Ph.D. degree from the University of Bradford, Bradford, U.K. From 2018 to 2020, he worked as a Marie Curie Research Fellow in the H2020-ITN-SECRET project funded by EU Commission, targeting 5G mobile small cells. From 2014 to 2018, he had worked with Antennas, propagation, and mm-Wave systems (APMS) Section, Aalborg University, Aalborg, Denmark. He has over 12 years' research experience in antenna and microwave engineering. He has authored or coauthored more than 300 journal and conference papers. His articles have more than 4750 citations with 37 h-index, reported by the Google Scholar. He is currently a Research Assistant and a Staff Member at the Faculty of Engineering and Informatics, University of Bradford, working as a Research Fellow in the SATNEX-V project, funded by the European Space Agency. Dr. Parchin was a recipient and a co-recipient of several awards for research publications such as Research Development Fund, MDPI Travel Award, and Best Paper Awards at URSI Symposium 2019 and U.K. URSI festival 2020. He is also a member and a Reviewer for various high-ranking journals and publishers such as IEEE Transactions, IEEE ACCESS/Letters, IET, Wiley, Springer, Elsevier, and MDPI.

 **Issa Elfergani** obtained his M.Sc. and Ph.D. degrees in electrical and electronic engineering from University of Bradford, UK, in 2008 and 2013, respectively. After his Ph.D. since 2013, he was working as "Postdoctoral Researcher" and then as "Investigador junior" at Instituto de Telecomunicações Aveiro, Portugal within the Mobile Systems group. In 2014 Issa received prestigious FCT fellowship for his postdoctoral research. The evaluation of the first triennium of this scholarship was given an excellent rating by the evaluators. He is now a senior researcher at the Instituto de Telecomunicações, Aveiro (Portugal), working with European research-funded projects, while while leading technical activities in antenna design for ENIAC ARTEMOS (2011–2014), EUREKA BENEFIC (2014–2017), CORTIF (2014–2017), GREEN-T (2011–2014), VALUE (2016–2016), THINGS2DO (2014–2018) and H2020-ITN-SECRET (2017–2020). To the present, all projects have been successfully concluded. He is currently working on (5GWAR) Novel 5G Millimetre-Wave Array Antennas for Future Mobile Handset Applications as Principle Investigator. Issa is the Guest editor/special issue of Electronics "Recent Technical Developments in Energy- Efficient 5G Mobile Cells ,Special Issue on Recent Advances in Engineering Systems Journal (ASTESJ) and Guest Editor/special issue of Electronics " Recent Advances in Antenna Design for 5G Heterogeneous Networks. Issa has around 145 high-impact publications in international conferences, journal papers, and book/book chapters with a google scholar h-index 18.

 **Jonathan Rodriguez** received his Master's degree in Electronic and Electrical Engineering and Ph.D from the University of Surrey (UK), in 1998 and 2004 respectively. In 2005, he became a researcher at the Instituto de Telecomunicações (Portugal) and Senior Researcher in 2008 where he established the Mobile System Research Group. He has served as project coordinator for major international research projects, including Eureka LOOP and FP7 C2POWER whilst serving as technical manager for FP7 COGEU and FP7 SALUS. He is currently the coordinator of the H2020-SECRET Innovative Training Network. Since 2009 he has served as Invited Assistant Professor at the University of Aveiro (Portugal), and attained Associate Level in 2015. In 2017 he was appointed Professor of Mobile Communications at the University of South Wales (UK). He is author of more than 500 scientific works, including 10 book editorials.

 **James Noras** is currently a Senior Lecturer with the School of Engineering, Design and Technology, University of Bradford, U.K. He is also the Director of five internationally franchised B.Eng. and M.Sc. courses in electrical and electronic engineering, has successfully supervised 18 Ph.D. students, and is currently supervising the research of 3 Ph.D. students. He has published 50 journal papers and 85 conference papers, in fundamental semiconductor physics, analog and digital circuit design, digital signal processing, and RF system design and evaluation. His main research interests include digital system design and implementation, DSP and coding for communication systems, and localization algorithms for mobile systems. He is a member of the Institute of Physics and a Chartered Physicist.

 **Raed Abd-Alhameed** (M'02, SM'13) is currently a Professor of electromagnetic and radiofrequency engineering with the University of Bradford, U.K. He is also the Leader of radiofrequency, propagation, sensor design, and signal processing; in addition to leading the Communications Research Group for years within the School of Engineering and Informatics, University of Bradford. He has long years' research experience in the areas of radio frequency, signal processing, propagations, antennas, and electromagnetic computational techniques. He has published over 800 academic journals and conference papers; in addition, he has co-authored six books and several book chapters including seven patents. He is a principal investigator for several funded applications to EPSRCs and the leader of several successful knowledge Transfer Programmes, such as with Arris (previously known as Pace plc), Yorkshire Water plc, Harvard Engineering plc, IETG Ltd., Seven Technologies Group, Emkay

Ltd., and Two World Ltd. He has also been a co-investigator in several funded research projects including 1) Horizon 2020 Research and Innovation programme under grant agreement H2020-MSCA-RISE-2019-eBORDER-872878; 2) H2020 MARIE Sk^{a}odowska-CURIE ACTIONS: Innovative Training Networks Secure Network Coding for Next Generation Mobile Small Cells 5G-US; 3) European Space Agency: Satellite Network of Experts V, Work Item 2.6: Frequency selectivity in phase-only beamformed user terminal direct radiating arrays; 4) Nonlinear and demodulation mechanisms in biological tissue (Dept. of Health, Mobile Telecommunications & Health Research Programme; and 5) Assessment of the Potential Direct Effects of Cellular Phones on the Nervous System (EU: collaboration with six other major research organizations across Europe). He was a recipient of the Business Innovation Award for his successful KTP with Pace and Datong companies on the design and implementation of MIMO sensor systems and antenna array design for service localizations. He is the chair of several successful workshops on energy-efficient and reconfigurable transceivers: Approach toward Energy Conservation and CO2 Reduction that addresses the biggest challenges for the future wireless systems. He is a co-editor for Electronics MDPI Journal since June 2019; in addition, he was a Guest Editor of IET Science, Measurements and Technology Journal since 2009. He has been a Research Visitor of Wrexham University, Wales, since 2009, covering the wireless and communications research areas. His interest in computational methods and optimizations, wireless and mobile communications, sensor design, EMC, beam steering antennas, energy-efficient PAs, and RF predistorter design applications. He is a fellow of the Institution of Engineering and Technology and a fellow of the Higher Education Academy and a Chartered Engineer.

Dr Ashwain Rayit was born in Bham, India, in 1965. After emigrating to England in 1972, he received the BEng degree in Electrical & Electronic Engineering from the University of Leeds, UK in 1987, and the MSc and Ph.D. degrees in Microwave Engineering from the University of Bradford, UK in 1989 and 1993, respectively. In 1993, he joined Filtronic Ltd as a RF Engineer, and in 1995 became instrumental in setting up Filtronic Cable Communications Ltd. He developed a range of amplifier and filtering products for the cable market, before leaving Filtronic and setting up his own business, SARAS Technology Limited, with his brother Dr Raj Rayit. SARAS Technology is involved with the design and manufacture of a range of products (Amplifiers/Filters/ TR/TX modules/RF Front Ends) for many markets including, Defence, Wireless Comms, Telecoms, Security & Surveillance. He has written numerous papers and contributed to a number of books. He has been a member of the IEEE and the IEE.

Rami Qahwaji is a Professor of Visual Computing at the University of Bradford. Rami is originally trained as an Electrical Engineer and had MSc in Control and Computer Engineering and PhD in AI and signal/image processing. He has been working with

different industries in the fields of satellite/space imaging, communications, remote sensing, digital health and imaging, Biometrics, AI and data visualisation developing intelligent systems in collaboration with NASA, ESA, NHS and different SMEs. Rami is a Fellow of the Institution of Engineering and Technology (FIET), Charted Engineer (CEng), Fellow of the Higher Education Academy (FHEA), IET technical assessor and sets on the IET's Healthcare Sector Executive Committee. Rami attracted millions of pounds in research funding from various UK and European funding agencies. He has over 140 refereed Journal and Conference publications and has been invited to deliver many keynote speeches at national and international conferences. He has supervised 31 completed PhD projects and is an external examiner for several UK and international universities. He is heavily involved in the organisation of international activities and public engagement events